Journal of Power Sources 196 (2011) 7931–7936

Contents lists available at ScienceDirect

Journal of Power Sources

journal homepage: www.elsevier.com/locate/jpowsour

# A highly stable $TiB_2$-supported Pt catalyst for polymer electrolyte membrane fuel cells

Shibin Yin[a,b], Shichun Mu[a,*], Mu Pan[a], Zhengyi Fu[a]

[a] State Key Laboratory of Advanced Technology for Materials Synthesis and Processing, Wuhan University of Technology, Wuhan 430070, PR China
[b] Low Carbon Energy Institute, China University of Mining and Technology, Xuzhou 221116, PR China

ARTICLE INFO

*Article history:*
Received 11 April 2011
Received in revised form 12 May 2011
Accepted 14 May 2011
Available online 27 May 2011

*Keywords:*
Catalysts
$TiB_2$
Perfluorosulfonic acid
Stability
Polymer electrolyte membrane fuel cells

ABSTRACT

Pt nanoparticles supported on $TiB_2$ conductive ceramics (Pt/$TiB_2$) have been prepared through a liquid reduction method, where the $TiB_2$ surfaces are stabilized with perfluorosulfonic acid. The prepared Pt/$TiB_2$ catalyst is characterized with X-ray diffraction (XRD) and TEM techniques, and a rotating disk electrode (RDE) apparatus. The Pt nanoparticles are found to uniformly disperse on the surface of the $TiB_2$ particles with narrow size distribution. The electrochemical stability of Pt/$TiB_2$ is evaluated and found highly electrochemically stable compared to a commercial Pt/C catalyst. Meanwhile, the catalyst also shows comparable performance for oxygen reduction reaction (ORR) to the Pt/C. The mechanism of the remarkable stability and comparable activity for ORR on Pt/$TiB_2$ is also proposed and discussed.


## 1. Introduction

Catalyst stability is long regarded as one of the most important critical success factors for the commercialization of proton exchange membrane fuel cells (PEMFCs) [1,2]. It is, therefore, highly desired to develop catalysts with good stability besides high performance. Despite their compromised stability, Pt/C and its alloys are still the most widely used catalysts materials that provide satisfactory performance for electrode reactions due to lacking of alternatives.

Changes in the catalysts and membrane electrode assembly (MEA) [3] and operating conditions [4], including the thermal [5,6] and humidity [7] during the operation of fuel cells, are known to influence the stability of conventional Pt/C catalysts. Carbon could be corroded in these circumstances, and the presence of Pt exacerbates the corrosion through accelerating the corrosion of carbon [8]. Irreversibly, the corrosion of carbon leads to the detachment of Pt [9], thus dramatically reducing the stability of Pt/C catalysts.

In order to improve the activity and stability of the catalysts for PEMFCs, numerous efforts have been reported. Examples included the use of newly prepared Pt nanocrystals in Pt/C catalysts [10], improvement in their preparation method [11–14], and syntheses of Pt dual or ternary alloys with Pd, Au, Ru, Re, Ir, Os, Fe, Co, Ni, Cr, Zn, and Mo [8,15–19]. Meanwhile, Pt alloyed with early transition metals, such as Sc and Y, reportedly showed improved activity toward oxygen reduction reaction (ORR) than pure Pt [20]. On the other hand, non-noble metal catalysts, such as Co–N–C or Fe–N–C, have also been intensively studied for oxygen reduction [21–23], which have attracted growing interest as substitutes for Pt, although none of them has yet met the stability requirements. With limited success, several carbon-like supports with high degree of graphitization [24] or with special pore structures [25] were employed to enhance the interaction between Pt nanoparticles and supports, such as CNT [26,27], CNF [28], porous carbon [25,29], carbon aerogel [30], and graphene [24].

In recent years, as the importance of stability for the commercialization of fuel cells gains increasing recognition, numerous ceramics or oxide-contain composites have been studied as catalysts supports, such as ITO [31], $WO_3$ [32], $TiO_2$ [33], $CeO_2$ [34], WC [14], $Ti_4O_7$ [35], $NbO_2$ or $Nb_2O_5$ [36], $CeO_2$–$ZrO_2$ [37], TiN [38], and SiC [39]. However, no ceramics has yet reported to possess good stability and, simultaneously, excellent conductivity at room temperature in acidic electrolyte. In order to make the conductive ceramics more attractive for PEMFCs, approaches such as intermingle with carbon [14,39] or modified with metal [40] were employed with, unfortunately, very limited success.

Widely used as cutting tools, titanium diboride ($TiB_2$), on the other hand, is commercially available with a high melting point, excellent thermal stability/corrosion resistance in acidic medium, and good electrical and high thermal conductivities [41,42], all of which are highly desired for harsh environments as in PEMFCs.

* Corresponding author. Tel.: +86 27 87651837; fax: +86 27 87879468.
*E-mail addresses:* msc@whut.edu.cn, mushichun@gmail.com (S. Mu).

0378-7753/$ – see front matter © 2011 Elsevier B.V. All rights reserved.
doi:10.1016/j.jpowsour.2011.05.033

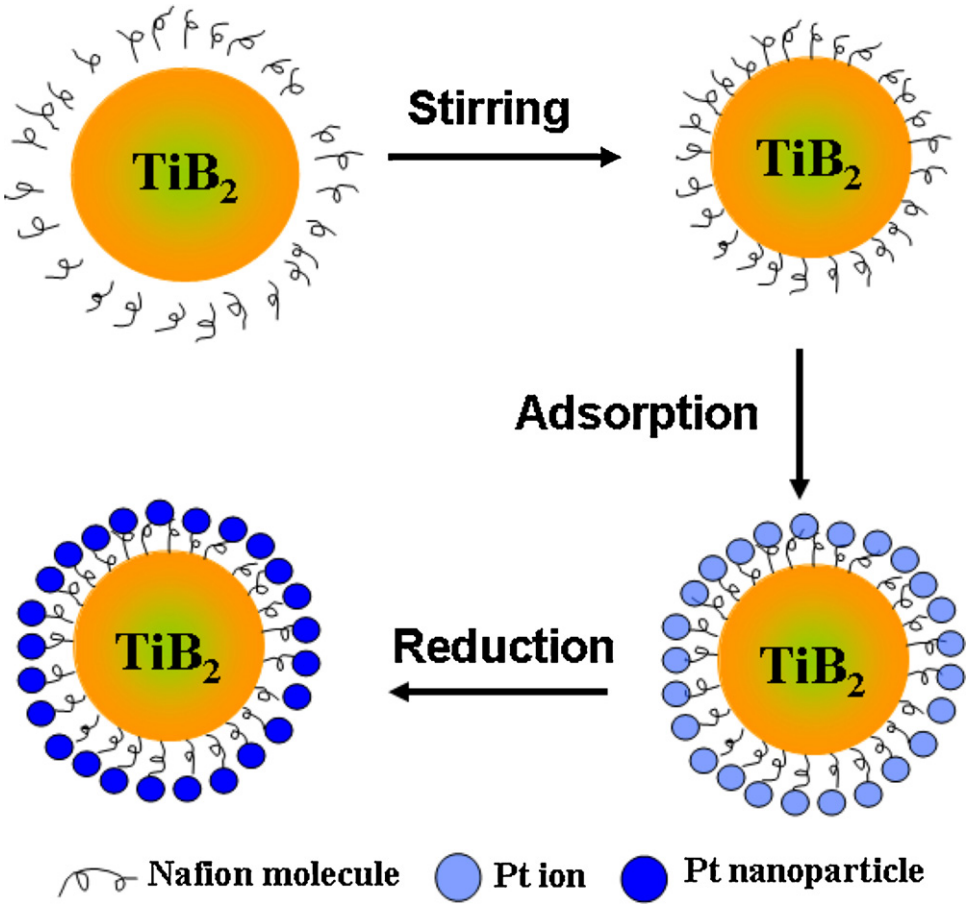


**Fig. 1.** Schematic of the preparation route to the $Pt/TiB_2$ catalysts.

However, Pt nanoparticles are difficult to deposit on the surface of $TiB_2$ particles, due primarily to the inertness of $TiB_2$. In our previous report [43], Pt nanoparticles were stabilized with perfluorosulfonic acid, and subsequently a $Pt/TiB_2$ catalyst was obtained through the adsorption of as-received Pt nano-colloids on bare $TiB_2$ surfaces. The perfluorosulfonic acid (Nafion®)-stabilized Pt nanoparticles supported on $TiB_2$ exhibited good stability for electrochemical oxidation and comparable performance for ORR to the Pt/C catalysts. In this work, the perfluorosulfonic acid serving as both a proton-conducting polymer and a stabilizer is employed to stabilize the surface of $TiB_2$ before coating Pt nanoparticles. Here the perfluorosulfonic acid-stabilized ceramic surfaces presumably enhance the interactions between the Pt particles and $TiB_2$ support as well as significantly improve the dispersion of Pt nanoparticles on the inert ceramic supports. The corresponding physical and chemical properties of the as-prepared catalyst are investigated using XRD, FTIR, TEM, and cyclic voltammetry (CV). The mechanism of the great stability observed in the catalysts is also proposed and discussed.

## 2. Experimental

### 2.1. Preparation of the $Pt/TiB_2$ catalyst

$TiB_2$ ultra-fine powders were prepared through the self-propagating high-temperature synthesis (SHS) method [41]. The schematic diagram of the catalyst preparation process is summarized in Fig. 1, and the steps are as follows. To a round bottom flask, ethanol (300 mL), deionized water (300 mL, Barbstead Nanopure, ≥18.30 MΩ $cm^{-1}$), and perfluorosulfonic acid Nafion (5.0 mL, 5.0 wt.%, DuPont Co., USA) were added sequentially. $TiB_2$ (0.49 g) was added to ethanol (20.0 mL) in a beaker, and the mixture was ultrasonically stirred for 10 min before it was charged dropwise into the above round bottom flask. Under vigorously stirring for 3 h at room temperature, Nafion stabilized $TiB_2$ powders were obtained. Subsequently, $H_2PtCl_6{\cdot}6H_2O$ (0.36 g, Sinopharm Chemical Reagent Co. Ltd, China) as a precursor was added to the reaction mixture, and kept stirring for 10 min. The mixture was then heated to 80 °C in a water bath. A sodium hydroxide solution (2.0 mol $L^{-1}$) was used to adjust the mixture pH to around 9.0, and the reaction mixture was refluxed for 1–2 h until the color of the solution turned from grey to dark. After the reaction mixture was allowed to cool down to room temperature, black solid precipitation was obtained. It was next filtered, washed, and dried at 80 °C for 12 h in a vacuum oven to give the final catalysts (denoted $Pt/TiB_2$). The Pt content in the catalyst was measured at 19.2 wt.% with inductively coupled plasma atomic emission spectroscopy (ICP-AES, PerkinElmer, Germany).

### 2.2. Catalysts characterization

XRD measurements were carried out on a D/Max-III (Rigaku Co., Japan) using Cu Ka radiation (λ = 0.15406 nm), and operated at 40 kV and 30 mA. The average crystal size of Pt nanoparticles was calculated according to the Scherrer formula [44,45]. Infrared spectroscopy was employed to detect the presence of Nafion that served as a cohesive agent between the Pt nanoparticles and $TiB_2$ substrate in the $Pt/TiB_2$ catalyst on a Fourier transform infrared spectrometer (Nicolet MAGNA-IR 560, FTIR, USA). A Nafion reference sample was prepared through evaporating 5.0 wt.% Nafion liquid (DuPont Co., USA). TEM images were taken on a JEOL JEM-2010 (HR) at 200 kV to analyze the particle size distribution of the Pt nanoparticles of

the $Pt/TiB_2$ catalysts. Histograms of the Pt nanoparticle distribution were prepared through measuring more than 300 particles.

An electrochemical accelerated stability test (ADT) was employed to evaluate the stability of the $Pt/TiB_2$ catalysts, as it is an inexpensive yet quick method to screen catalysts for stability and performance. A CV method instead of a chronoamperometry or chronopotentiometry method was employed to conduct ADT, simply because the former is more efficient and closely related to the actual operating conditions [46,47] than the other two.

Electrochemical measurements were carried out on an Autolab PGSTAT 30 potentiostat (Eco Chemie B.V., Holand) instrument in a thermostat-controlled standard three-electrode cell at room temperature using an $Hg/Hg_2SO_4$ electrode and a platinum foil (1.0 cm × 1.0 cm) as a reference and counter electrodes. A glass carbon (GC) disk electrode (∅ = 4.0 mm) was used as the substrate for the catalysts thin film in the electrochemical measurements. The thin film catalysts working electrode was prepared as follows: the $Pt/TiB_2$ catalysts was placed in deionized water (500.0 μL) before being treated with a Nafion solution (21.0 μL, 5.0 wt.%). The solution was next dispersed in an ultrasonic bar for 10 min to obtain a well-dispersed catalyst ink, which was quantitatively transferred onto the surface of the GC electrode using a micropipette, and dried under an infrared lamp to yield the catalyst thin film. The catalyst loading was kept constant at 0.40 mg $cm^{-2}$ for the catalyst investigated in this study. CVs were carried out in $H_2SO_4$ aqueous solutions (0.5 mol $L^{-1}$) that were deaerated with high-purity nitrogen gas prior to use. ADT was conducted with CVs between 0.6 and 1.20 V, and all CV curves were recorded from 0 to 1.20 V at a scan rate of 20 mV $s^{-1}$ before and after ADT. The electrochemical surface areas (ESA, $m^2\ g^{-1}$ Pt) of the catalysts were calculated from the integrated charge in the hydrogen adsorption peak area of the CV curves [48]. ESA was calculated from Eq. (1) with the Pt poly-crystallite hydrogen adsorptions constant of 210 μC $cm^{-2}$ Pt.

$$S_{ESA}\left[\frac{m^2\ Pt}{g\ Pt}\right] = \frac{\text{charge}[\mu C\ cm^{-2}]}{210[\mu C\ cm^{-2}\ Pt] \times Pt\ \text{loading}[mg\ cm^{-2}]} \times 10 \quad (1)$$

In addition, the ORR performance of $Pt/TiB_2$ was evaluated with the use of a rotating disk electrode (RDE) apparatus in $H_2SO_4$ aqueous solutions (0.5 mol $L^{-1}$, oxygen saturated) at a sweep rate of 10 mV $s^{-1}$ and a speed of 1600 rpm at room temperature, recorded from 1.1 to 0 V. All measured potentials were referred to the reversible hydrogen electrode (RHE) without specification.

## 3. Results and discussion

As shown in the XRD spectrum in Fig. 2, it is apparent that the (1 0 2) peak of $TiB_2$ overlaps with Pt (2 2 0), and the (1 0 1) peak of $TiB_2$ is very close to Pt (2 0 0). Therefore, only the peak of Pt (1 1 1) can be used to calculate the average crystal size of Pt, and the average crystal size of the Pt nanoparticles calculated using the Debye–Scherrer formula [44,45] is 3.4 nm.

FTIR spectra of Nafion and the $Pt/TiB_2$ catalyst are given in Fig. 3. For the $Pt/TiB_2$ catalyst, the relatively strong characteristic band at 1279 $cm^{-1}$ could be assigned to $-CF_2$ stretching vibration, corresponding to the bands at 1238 $cm^{-1}$ in Nafion. The other relatively weak band at 991 $cm^{-1}$ might be associated with the C–O–C symmetric stretching vibration, corresponding to the band at 983 $cm^{-1}$ in Nafion. These results indicate the presence of Nafion molecule in the as-prepared $Pt/TiB_2$ catalyst.

Revealed in Fig. 4(a) and (b) are the TEM images of the $Pt/TiB_2$ catalysts. According to these TEM images, Pt nanoparticles are homogeneously dispersed on the surface of $TiB_2$ particles with no obvious agglomeration. It is interesting that the Pt nanoparticles adopt flocculent monodisperse, which is very different from the monoparticle disperse of Pt on pristine supports, such as carbon black [26,39,43]. This unique distribution of Pt particles can be attributed to the effect of Nafion covered on the support surfaces as a stabilizer, facilitating increase in the Pt particle number in a unit area. Accordingly, the average particle size of Pt nanoparticles is about 3.1 nm obtained from several random areas in the TEM images containing more than 300 particles (Fig. 4(c)), which is comparable to commercial Pt/C catalysts [43]. In addition, the selected-area EDAX analyses of catalyst surfaces have been investigated (Fig. 4(b) and (d)). The presence of Nafion as a stabilizer in the $Pt/TiB_2$ catalyst is evidenced by the measurement of elements C, F, and S that form PFSA Nafion.

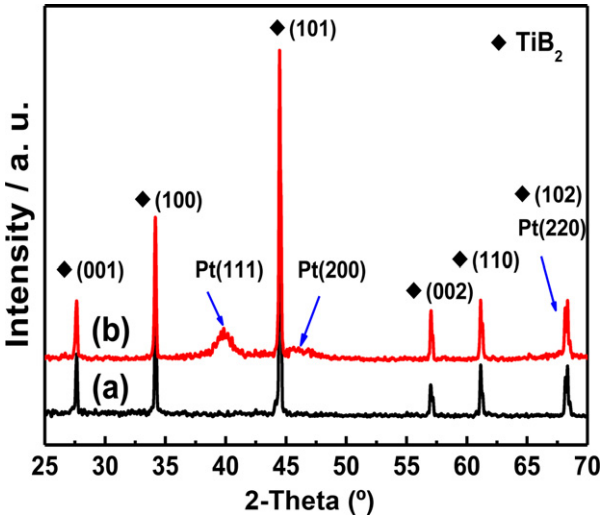


**Fig. 2.** XRD pattern of the $TiB_2$ (a) and $Pt/TiB_2$ (b) catalysts.

The initial and final CVs of the $Pt/TiB_2$ catalyst during ADT are compared in Fig. 5(a). The initial ESA of $Pt/TiB_2$ is 37.5 $m^2\ g^{-1}$, which is lower than 61.4 $m^2\ g^{-1}$ observed in a commercial 20 wt.% Pt/C catalyst (Johnson Matthey, USA) as shown in Fig. 5(b). Such small ESA could be attributed to the relative large particle size and high density of the $TiB_2$ powders compared to the carbon support, as well as the likely occupancy of Nafion molecules on the surface of Pt. However, an improvement in the ORR activity is observed for $Pt/TiB_2$ as evidenced by the onset potential. $Pt/TiB_2$ shows a higher reduction current of 0.30 mA $cm^{-2}$ at 0.9 V as compared to

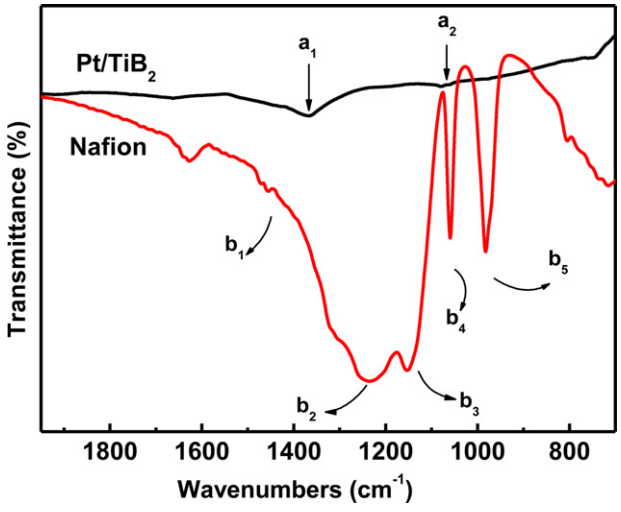


**Fig. 3.** FTIR spectra of Nafion and the $Pt/TiB_2$ catalysts. The bands at $b_1$, $b_2$, $b_3$, $b_4$ and $b_5$ are assigned to S=O asymmetric stretching ($-SO_2OH$ group), $CF_2$ asymmetric stretching, $CF_2$ symmetric stretching, S–O symmetric stretching ($-SO_3^-$ ion), and C–O–C symmetric stretching of Nafion, respectively.

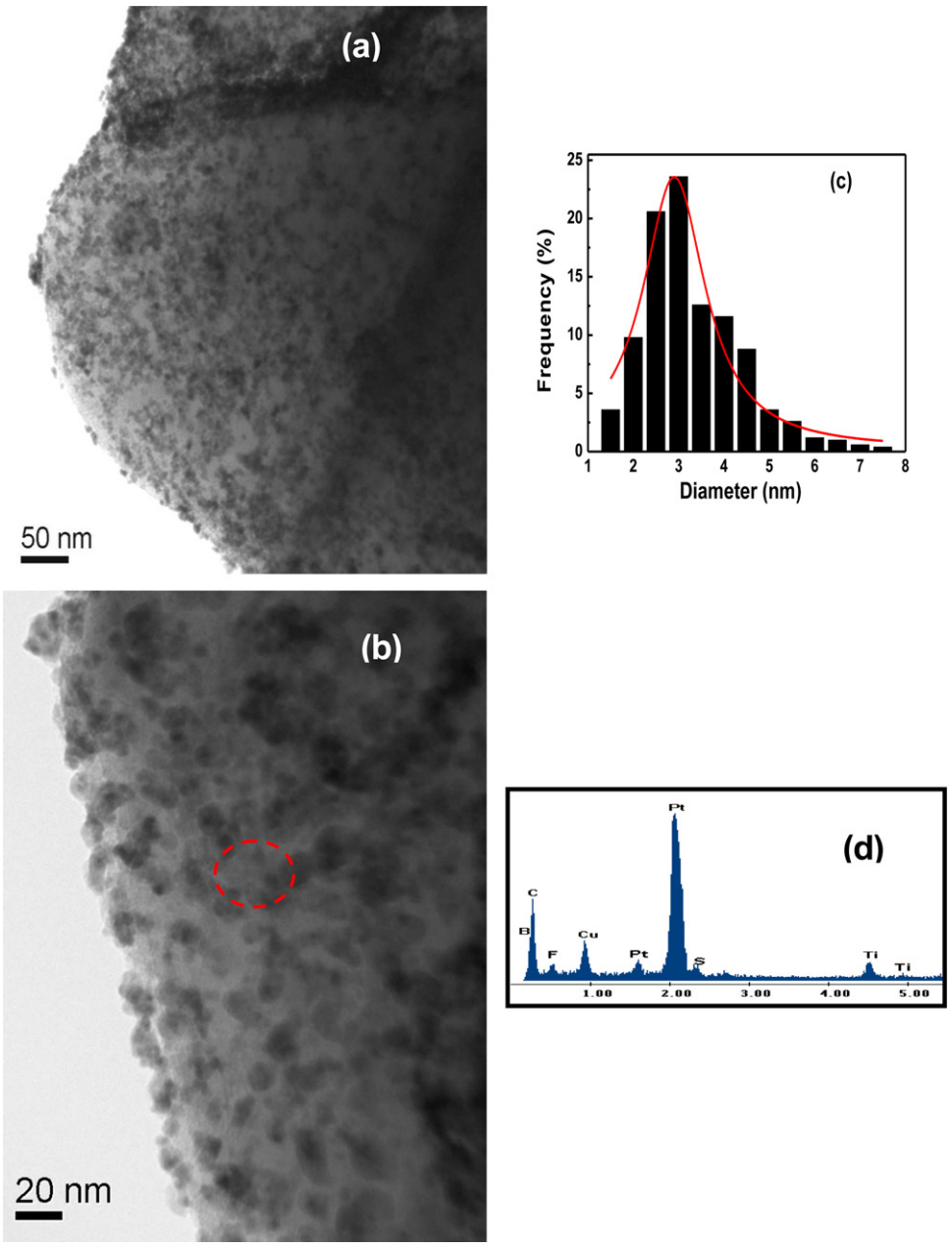


**Fig. 4.** TEM images of the $Pt/TiB_2$ catalyst with varied scale bars (a and b) and corresponding particle size distribution histograms of Pt nanoparticles (c), and the selected-area EDAX of the $Pt/TiB_2$ catalyst shown in image b (d).

0.12 mA $cm^{-2}$ at 0.9 V found in the Pt/C catalyst with the same Pt loading as shown in Fig. 5(c). In our previous study [43], the same trends were observed in a Nafion modified Pt catalyst on a $TiB_2$ support. Similar results were also reported by Avasarala et al. [38], who demonstrated that TiN-supported Pt catalysts had better performance for the oxygen reduction reaction in comparison with carbon supported catalysts. These findings further suggest that activity improvement in $Pt/TiB_2$ is attributed to the influence of support materials [14,38,43]. Therefore, the conductive ceramics, serving as the support for Pt catalysts, help enhance their electrocatalytic activity. Additionally, our experimental results indicate that Nafion layers have a negligible effect on the outer surfaces of $TiB_2$. In fact, our previous study [49,50] showed that the transfer process of reaction species during ORR was mediated by $-SO_3^-$ functional groups in the polyelectrolyte chain structure of Nafion, thus increasing the three-phase reaction boundary in PEM fuel cell electrodes.

Fig. 5(d) shows the ESA loss of Pt in the function of potential cycle numbers. ESA of the Pt/C catalyst decreases rapidly with increasing cycle numbers. However, the ESA loss for $Pt/TiB_2$ is slow compared to the Pt/C catalyst. The ESA loss rate of Pt/C reaches $1.54 \times 10^{-2}$ $m^2$ $g^{-1}$ $cycle^{-1}$, whereas $Pt/TiB_2$ has only $3.00 \times 10^{-3}$ $m^2$ $g^{-1}$ $cycle^{-1}$, which is 5.1 times lower than Pt/C, indicating that $Pt/TiB_2$ has an approximately five times longer lifetime than Pt/C under the conditions of an electrochemical acceleration. The ESA loss of Pt/C is also visibly higher than that of $Pt/TiB_2$, where the perfluorosulfonic acid-stabilized Pt nanoparticles are supported on $TiB_2$ (approximately four times longer lifetime than Pt/C) [43], indicating the perfluorosulfonic acid-stabilized supports may be more favorable than the perfluorosulfonic acid-stabilized Pt nanoparticles to improve the catalyst lifetime for such polymer-stabilized $Pt/TiB_2$ catalyst.

The smaller the particle size is, usually the easier the particles agglomerate due to their high surface activation energy [51]. The

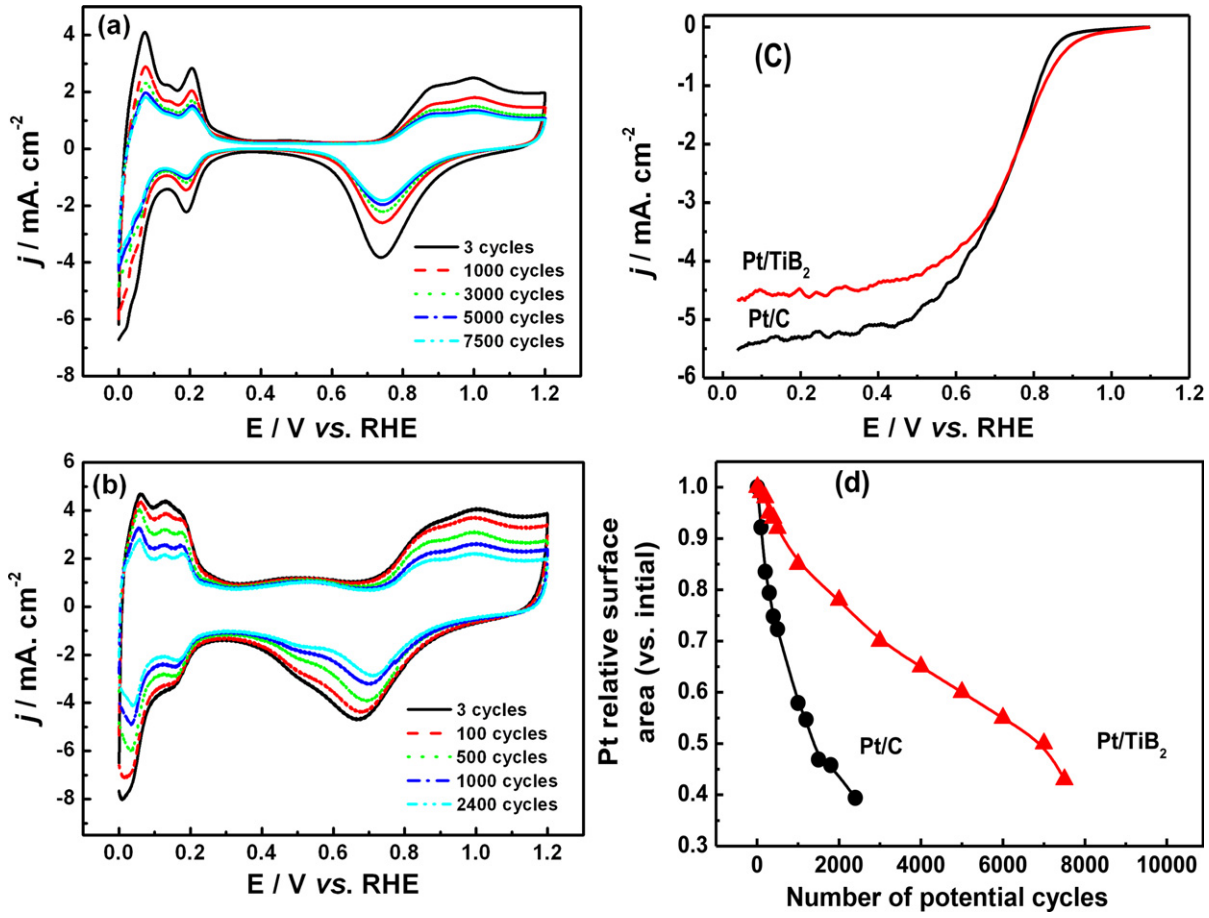


**Fig. 5.** CV curves of $Pt/TiB_2$ (a) and a commercial 20 wt.% Pt/C catalysts (b) under accelerated durability tests in $H_2SO_4$ aqueous solutions (0.5 mol $L^{-1}$), at scan rate of 20 mV $s^{-1}$ and temperature of 25 °C. (c) Oxygen reduction reaction on the $Pt/TiB_2$ and Pt/C catalysts in $H_2SO_4$ aqueous solutions (0.5 mol $L^{-1}$, oxygen saturated) at 25 °C, at a scan rate of 10 mV $s^{-1}$ and a speed of 1600 rpm. (d) Changes in the electrochemical surface area (ESA) of the catalysts related to Pt catalytic surface area with increasing potential cycles.

Pt particle sizes in both catalysts are in the range of 3.0 nm, giving the Pt nanoparticles strong tendency of agglomeration, and thus leading to ESA loss. Meanwhile, the carbon support could be corroded during long-term operation [52], and such corrosion is likely exacerbated especially in the presence of Pt [8,9]. As such, the interaction between the carbon and Pt nanoparticles weakens, and the Pt nanoparticles would collapse into the carbon-deficient XC-72 support, consequently accelerating the agglomeration of the Pt nanoparticles. Meantime, decrease in the Pt nanoparticles could also be attributed to the Ostwald ripening [53]. In contrast, $TiB_2$ supports are highly electrochemically stable relative to carbon supports [43], endowing Pt nanoparticles on $TiB_2$ supports with higher stability and less reduction than those on carbon supports.

As far as the migration of Pt nanoparticles on a support is concerned, we tend to believe that it is dependent on the Pt-support interaction and steric hindrance from the Nafion functional groups. The Pt nanoparticles stabilized with Nafion in $Pt/TiB_2$ have both electron rich $-SO_3$ groups in Nafion and highly electron deficient surface of $TiB_2$, creating strong adhesion between the Pt and support surface that increases their interactions. The Pt nanoparticles are, therefore, tightly anchored on the $TiB_2$ surface. Besides, the Nafion layers increase the roughness of the $TiB_2$ surface, effecting more strong steric hindrance than that of pure Pt nanoparticles. The resistance to Pt nanoparticles migration is thus greatly enhanced.

Fig. 6 presents two migration models of Pt nanoparticles stabilized with Nafion on the $TiB_2$ surface. Pt nanoparticles are presumably mainly driven by periodic changeable electric field force ($f_1$) during ADT, and Pt nanoparticles only moves when $f_1$ is greater than the friction resistance ($f_2$) between the Pt nanoparticles and Nafion modified $TiB_2$ powders. The Pt nanoparticles should have high resistance to migration because of the strong Pt-supports interaction. Therefore, the aggregation of Pt nanoparticles is rather difficult. When $f_1$ is insufficient magnitude relative to $f_2$ as shown in Fig. 6(a), the migration and aggregation of Pt nanoparticles take place, although the aggregation is hindered by the Nafion polymer layer distributed on the $TiB_2$ surface, and it only occurs when Nafion is decomposed after long-term electrochemical oxidation.

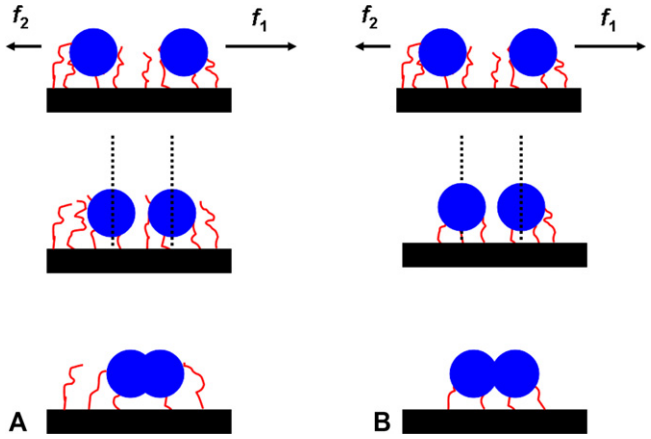


**Fig. 6.** Schematic of the migration model of Pt nanoparticles moving on the catalyst support. (a) Migration of Pt colloid particles driven by an electric field force, and (b) migration of Pt nanoparticles coupled with Nafion polymer oxidization.

When the electric field force ($f_1$) is below sufficient magnitude, as shown in Fig. 6(b), no migration of Pt nanoparticles occurs. However, Nafion decomposes gradually with the time, leading to decrease in resistance to particle migration. Once the critical moving force is reached, Pt nanoparticles will start to move on the support surface, and thus gather toward each other. In this case, Pt nanoparticles aggregate due to the absence of protection from the integrated Nafion polymer layer on the $TiB_2$ surface.

## 4. Conclusions

A Pt/$TiB_2$ catalyst for PEM fuel cells with high stability has been prepared and studied. The catalyst prepared with Pt loaded on perfluorosulfonic acid Nafion- stabilized $TiB_2$ particles displays an improved activity in the oxygen reduction reaction and remarkably high electrochemical stability. The Pt/$TiB_2$ catalyst is much more stable than that of a commercial Pt/C catalyst, which is likely attributed to the excellent stability of the $TiB_2$ support and the stabilization effect from Nafion. The current study shows great promises for Pt/$TiB_2$ catalysts as an alternative to commercial Pt/C catalysts.

## Acknowledgements

This work was financially supported by the National Natural Science Foundation of China (NSFC, nos. 50972112 and 50632050), the New Century Excellent Talent Program of Ministry of Education of China (MOE) (no. NCET-07-0652), and Fundamental Research Funds for the Central Universities.

## References

[1] S.S. Zhang, X.Z. Yuan, H.J. Wang, W. Merida, H. Zhu, J. Shen, S.H. Wu, J.J. Zhang, Int. J. Hydrogen Energy 34 (2009) 388.
[2] Y.H. Bing, H.S. Liu, L. Zhang, D. Ghosh, J.J. Zhang, Chem. Soc. Rev. 39 (2010) 2184.
[3] E. Antolini, J. Mater. Sci. 38 (2003) 2995.
[4] L.M. Roen, C.H. Paik, T.D. Jarvic, Electrochem. Solid-State Lett. 7 (2004) A19.
[5] D.A. Stevens, J.R. Dahn, Carbon 43 (2005) 179.
[6] K.H. Kangasniemi, D.A. Condit, T.D. Jarvi, J. Electrochem. Soc. 151 (2004) E125.
[7] J. Xie, D.L. Wood, D.M. Wayne, T.A. Zawodzinski, P. Atanassov, R.L. Borup, J. Electrochem. Soc. 152 (2005) A104.
[8] J. Zhang, K. Sasaki, E. Sutter, R.R. Adzic, Science 315 (2007) 220.
[9] Y.Y. Shao, G.P. Yin, Y.Z. Gao, J. Power Sources 171 (2007) 558.
[10] N. Tian, Z.Y. Zhou, S.G. Sun, Y. Ding, Z.L. Wang, Science 316 (2007) 732.
[11] Z.H. Zhou, S.L. Wang, W.J. Zhou, L.H. Jiang, G.X. Wang, G.Q. Sun, B. Zhou, Q. Xin, Phys. Chem. Chem. Phys. 5 (2003) 5485.
[12] Y.Y. Shao, G.P. Yin, J.J. Wang, Y.Z. Gao, P.F. Shi, J. Power Sources 161 (2006) 47.
[13] S.B. Yin, P.K. Shen, S.Q. Song, S.P. Jiang, Electrochim. Acta 54 (2009) 6954.
[14] P.K. Shen, S.B. Yin, Z.H. Li, C. Chen, Electrochim. Acta 55 (2010) 7969.
[15] B. Lim, M.J. Jiang, P.H.C. Camargo, E.C. Cho, J. Tao, X.M. Lu, Y.M. Zhu, Y.N. Xia, Science 324 (2009) 1302.
[16] J.X. Wang, H. Inada, L.J. Wu, Y.M. Zhu, Y.M. Choi, P. Liu, W.P. Zhou, R.R. Adzic, J. Am. Chem. Soc. 131 (2009) 17298.
[17] G.E. Ramirez-Caballero, Y.G. Ma, R. Callejas-Tovar, P.B. Balbuena, Phys. Chem. Chem. Phys. 12 (2010) 2209.
[18] V.R. Stamenkovic, B. Fowler, B.S. Mun, G.F. Wang, P.N. Ross, C.A. Lucas, N.M. Markovic, Science 315 (2007) 493.
[19] J.B. Wu, J.L. Zhang, Z.M. Peng, S.C. Yang, F.T. Wagner, H. Yang, J. Am. Chem. Soc. 132 (2010) 4984.
[20] J. Greeley, I.E.L. Stephens, A.S. Bondarenko, T.P. Johansson, H.A. Hansen, T.F. Jaramillo, J. Rossmeisl, I. Chorkendorff, J.K. Norskov, Nat. Chem. 1 (2009) 552.
[21] M. Lefevre, E. Proietti, F. Jaouen, J.P. Dodelet, Science 324 (2009) 71.
[22] H. Meng, F. Jaouen, E. Proietti, M. Lefevre, J.P. Dodelet, Electrochem. Commun. 11 (2009) 1986.
[23] C.W.B. Bezerra, L. Zhang, K.C. Lee, H.S. Liu, A.L.B. Marques, E.P. Marques, H.J. Wang, J.J. Zhang, Electrochim. Acta 53 (2008) 4937.
[24] L.T. Qu, Y. Liu, J.B. Baek, L.M. Dai, ACS Nano. 4 (2010) 1321.
[25] S.Q. Song, S.B. Yin, Z.H. Li, P.K. Shen, R.W. Fu, D.C. Wu, J. Power Sources 195 (2010) 1946.
[26] D.P. He, S.C. Mu, M. Pan, Carbon 49 (2011) 82.
[27] S. Zhang, Y.Y. Shao, G.P. Yin, Y.H. Lin, J. Mater. Chem. 20 (2010) 2826.
[28] J.S. Zheng, X.S. Zhang, P. Li, X.G. Zhou, W.K. Yuan, Catal. Today 131 (2008) 270.
[29] J.S. Yu, S. Kang, S.B. Yoon, G. Chai, J. Am. Chem. Soc. 124 (2002) 9382.
[30] A. Smirnova, X. Dong, H. Hara, A. Vasiliev, N. Sammes, Int. J. Hydrogen Energy 30 (2005) 149.
[31] H. Chhina, S. Campbell, O. Kesler, J. Power Sources 161 (2006) 893.
[32] J. Rajeswari, B. Viswanathan, T.K. Varadarajan, Mater. Chem. Phys. 106 (2007) 168.
[33] S. von Kraemer, J. Wikander, G. Lindbergh, A. Lundblad, A.E.C. Palmqvist, J. Power Sources 180 (2008) 185.
[34] H. Sakurai, T. Akita, S. Tsubota, M. Kiuchi, M. Haruta, Appl. Catal. A 291 (2005) 179.
[35] T. Ioroi, Z. Siroma, N. Fujiwara, S. Yamazaki, K. Yasuda, Electrochem. Commun. 7 (2005) 183.
[36] K. Sasaki, L. Zhang, R.R. Adzic, Phys. Chem. Chem. Phys. 10 (2008) 159.
[37] W. Ruettinger, X.S. Liu, R.J. Farrauto, Appl. Catal. B 65 (2006) 135.
[38] B. Avasarala, T. Murray, W.Z. Li, P. Haldar, J. Mater. Chem. 19 (2009) 1803.
[39] H.F. Lv, S.C. Mu, N.C. Cheng, M. Pan, Appl. Catal. B 100 (2010) 190.
[40] K.W. Park, K.S. Seol, Electrochem. Commun. 9 (2007) 2256.
[41] J.Y. Zhang, Z.Y. Fu, W.M. Wang, J. Mater. Sci. Technol. 21 (2005) 841.
[42] Z.Y. Fu, H. Wang, W.M. Wang, Q.J. Zheng, R.Z. Yuan, Key Eng. Mater. 217 (2002) 41.
[43] S.B. Yin, S.C. Mu, H.F. Lv, N.C. Cheng, M. Pan, Z.Y. Fu, Appl. Catal. B 93 (2010) 233.
[44] V. Radmilovic, H.A. Gasteiger, P.N. Ross, J. Catal. 154 (1995) 98.
[45] A.L. Patterson, Phys. Rev. 56 (1939) 978.
[46] X.P. Wang, R. Kumar, D.J. Myers, Electrochem. Solid-State Lett. 9 (2006) A225.
[47] C.H. Paik, G.S. Saloka, G.W. Graham, Electrochem. Solid-State Lett. 10 (2007) B39.
[48] Y. Xing, J. Phys. Chem. B 108 (2004) 19255.
[49] N.C. Cheng, S.C. Mu, M. Pan, P.P. Edwards, Electrochem. Commun. 11 (2009) 1610.
[50] N.C. Cheng, S.C. Mu, X.J. Chen, H.F. Lv, M. Pan, P.P. Edwards, Electrochim. Acta 56 (2011) 2154.
[51] J. Xie, D.L. Wood, K.L. More, P. Atanassov, R.L. Borup, J. Electrochem. Soc. 152 (2005) A1011.
[52] J.J. Wang, G.P. Yin, Y.Y. Shao, S. Zhang, Z.B. Wang, Y.Z. Gao, J. Power Sources 171 (2007) 331.
[53] A.V. Virkar, Y.K. Zhou, J. Electrochem. Soc. 154 (2007) B540.